7050 *Biochemistry* **2010,** *49,* 7050–7059
DOI: 10.1021/bi901969a

BIOCHEMISTRY
including biophysical chemistry & molecular biology
Article

Combinations of Affinity-Enhancing Mutations in a T Cell Receptor Reveal Highly Nonadditive Effects within and between Complementarity Determining Regions and Chains[†]

Brian G. Pierce,[‡,§] Jaafar N. Haidar,[∥,⊥] Yong Yu,[§,∥,@] and Zhiping Weng*[,‡,§,∥]

[‡]*Bioinformatics Program, Boston University, Boston, Massachusetts 02215,* [§]*Program in Bioinformatics and Integrative Biology, University of Massachusetts Medical School, Worcester, Massachusetts 01605, and* [∥]*Department of Biomedical Engineering, Boston University, Boston, Massachusetts 02215.* [⊥]*Present address: Imclone Systems, New York, NY 10014.* [@]*Present address: Novartis Institutes for Biomedical Research, Cambridge, MA 02139-4229.*

Received November 15, 2009; Revised Manuscript Received July 17, 2010

ABSTRACT: Understanding the energetic and structural response to multiple mutations in a protein−protein interface is a key aspect of rational protein design. Here we investigate the cooperativity of combinations of point mutations of a T cell receptor (TCR) that binds *in vivo* to HLA-A2 MHC and a viral peptide. The mutations were obtained from two sources: a structure-based design study on the TCR α chain (nine mutations) and an *in vitro* selection study on the TCR *β* chain (four mutations). In addition to combining the highest-affinity variants from each chain, we tested other combinations of mutations within and among the chains, for a total of 23 TCR mutants that we measured for binding kinetics to the peptide and major histocompatibility complex. A wide range of binding affinities was observed, from 2- to 1000-fold binding improvement versus that of the wild type, with significant nonadditive effects observed within and between TCR chains. This included an amino acid-dependent cooperative interaction between CDR1 and CDR3 residues that are separated by more than 9 Å in the wild-type complex. When analyzing the kinetics of the mutations, we found that the association rates were primarily responsible for the cooperativity, while the dissociation rates were responsible for the anticooperativity (less-than-additive energetics). On the basis of structural modeling of anticooperative mutants, we determined that side chain clash between proximal mutants likely led to nonadditive binding energies. These results highlight the complex nature of TCR association and binding and will be informative in future design efforts that combine multiple mutant residues.

Protein−protein interactions are responsible for a large variety of biological processes, including humoral and cellular immune responses, viral capsid assembly, and inhibition of enzyme function. While much progress has been made in understanding protein−protein interactions on a molecular and structural level, because of their enormous complexity there is still much to be learned before the dynamic interplay between residues in an interface is understood and can be modeled reliably.

One important area of protein−protein interaction research is the energetic and structural impact of multiple simultaneous mutations in a protein interface. Initial research in this area determined that the majority of combinations of mutations have additive energetics; however, nonadditivity is seen in cases where the interface is not rigid or the mutant residues are close to one another (*1*). On the basis of binding data from mutagenesis studies and protein structural data, some have found that protein interfaces are organized into a modular framework, with each module composed of a cluster of interacting residues that exhibit cooperative binding behavior (where the measured binding energy improvement, $\Delta\Delta G$, is larger than the sum of individual $\Delta\Delta G$ values), whereas separate modules act independently and have additive binding energetics (*2*−*4*). However, a recent study of combinations of mutations on a T cell receptor (TCR)[1] obtained from phage display in fact found significant cooperativity within and between modules (also termed hot regions) (*5*). The inter-hot spot cooperativity was exhibited between clusters separated by more than 20 Å; the authors attributed this to TCR flexibility and propagation of the energetics through a "dynamic structural network". Combinations of sets of mutations from multiple experiments have not been studied extensively, though one study found that when mutant modules of human growth hormone (hGH) from separate phage display experiments were combined, they behaved in a largely additive fashion (although there was cooperativity within the modules) (*6*). Rational design protocols have been utilized to improve the affinities of antibodies for antigens by combining point mutations, with the highest-affinity antibody mutants displaying additivity (*7*) and cooperativity (*8*) between point mutations.

In this study, we investigate the cooperative nature of protein binding by measuring the binding kinetics of combinations of point mutants in a TCR−peptide−MHC interface. This system

[†]This work was supported by National Institutes of Health Grant R01 GM084884 and National Science Foundation Grants DBI-0133834 and DBI-0116674 (to Z.W.).

*To whom correspondence should be addressed: University of Massachusetts Medical School, 364 Plantation St., Worcester, MA 01605. Telephone: (508) 856-8866. Fax: (508) 856-2392. E-mail: zhiping.weng@umassmed.edu.

[1]Abbreviations: TCR, T cell receptor; HLA, human leukocyte antigen; MHC, major histocompatibility complex; CDR, complementarity-determining region; SPR, surface plasmon resonance.

 Published on Web 07/19/2010

is of critical interest in immunology and vaccine design (*9*, *10*), as well as cell and antigen targeting (*11*). Several studies have featured improvement of the affinity of various TCRs for peptide−MHC complexes using *in vitro* selection methods, as discussed in several reviews (*12*−*14*). We produced mutations on the A6 TCR, which is a human αβ T cell receptor that binds *in vivo* to HLA-A2 MHC and a 9-mer peptide from the Tax protein of human T-lymphotropic virus 1 (HTLV-1). The structure of this complex has been determined by X-ray crystallography (*15*), and its binding kinetics and thermodynamics have been reported in several studies (*16*−*19*).

The mutations we selected for combination are from two sources: a phage display study that improved binding approximately 700-fold versus that of the wild type (*20*) and a structure-based design study we performed that improved binding approximately 100-fold versus that of the wild type (*19*). As the structure-based design mutants are located on the α chain and the phage display mutants are located on the β chain, we tested the combination of the two high-affinity mutant chains, as well as other combinations of mutations within and among the chains, leading to a total of 23 combinations of mutations that we produced and measured for peptide−MHC binding. While many of the combinations exhibited cooperativity and additivity, three had a significant degree of anticooperativity (also termed negative cooperativity), with measured energies lower than those expected from additivity of the component point mutations. We determined the contributions of specific residues to the nonadditive nature of the cooperative (and anticooperative) mutants, as well as the contributions of the association and dissociation rates. To further explore these experimental results, we performed an *in silico* analysis of the anticooperative mutations to determine their impact on the structure of the complex and found side chain clash between affinity-improving point mutations leading to anticooperativity.

MATERIALS AND METHODS

Energy Change Calculation. $\Delta\Delta G_{on}$ and $\Delta\Delta G_{off}$ were computed using the association rate (k_{on}) and dissocation rate (k_{off}) as follows:

$$\Delta\Delta G_{on} = RT \ln(k_{on\_wild\text{-}type}/k_{on\_mutant}) \quad (1)$$

$$\Delta\Delta G_{off} = RT \ln(k_{off\_mutant}/k_{off\_wild\text{-}type}) \quad (2)$$

In these equations, R is the gas constant and T is the temperature in kelvin. The total binding energy change, $\Delta\Delta G$, is the sum of these terms:

$$\begin{aligned}\Delta\Delta G &= RT \ln(K_{d\_mutant}/K_{d\_wild\text{-}type}) \\ &= RT \ln(k_{off\_mutant}k_{on\_wild\text{-}type}/k_{on\_mutant}k_{off\_wild\text{-}type}) \\ &= \Delta\Delta G_{on} + \Delta\Delta G_{off}\end{aligned} \quad (3)$$

where K_d is the equilibrium dissociation constant, equal to k_{off}/k_{on}.

Protein Expression and Purification. Proteins were expressed and purified as described previously by Haidar et al. (*19*). Briefly, mutations were introduced into the TCR constructs via site-directed mutagenesis using standard PCR protocols. HLA-A2, β2M, and wild-type and mutant TCRα and TCRβ chains were expressed separately as inclusion bodies in *Escherichia coli*. The inclusion bodies were refolded using protocols based on those of Garboczi et al. for TCRα and TCRβ (*21*), and for refolding the Tax peptide (LLFGYPVYV) with HLA-A2 and β2M to form the MHC−peptide complex (*22*). Fast protein liquid chromatography (FPLC) using a size exclusion column (rather than dialysis and ion exchange) was used to separate the folded proteins from aggregates, resulting in purification of the proteins that was faster than the previously published method (*21*).

Measurement of Binding Kinetics. Binding of wild-type and mutant TCRs to the Tax−HLA-A2 MHC complex was assessed using a Biacore 3000 surface plasmon resonance (SPR) biosensor at 25 °C. HBS-EP [0.01 M HEPES (pH 7.4), 0.15 mM NaCl, 3 mM EDTA, and 0.005% (v/v) Surfactant P20] was used as a running buffer during binding affinity measurements. Approximately 400 response units (RU) of TCR was immobilized onto a CM5 chip using the standard amine coupling procedure. The Tax−HLA-A2 complex was injected over immobilized TCR at a flow rate of 100 μL/min, followed by dissociation using running buffer. The injection time was either 90 or 150 s, with the latter time used to allow for adequate association of the high-affinity complexes. Tax−HLA-A2 complex concentrations were gradients of 2-fold dilutions, with at least three concentrations per gradient, and three gradients per experiment.

After dissociation, regeneration of the TCR surface was achieved with a single 2 min injection of 0.01 M HEPES (pH 7.4) and 1 M NaCl (for lower-affinity complexes, $K_d > 10^{-8}$) or two 10 s injections of 10 mM HCl (for high-affinity complexes, $K_d < 10^{-8}$). The latter regeneration condition was selected after testing the β chain **MSAQ** mutant from Li et al. (*20*) using the HEPES/NaCl solution; only one measurable concentration was obtained for kinetic analysis because of incomplete TCR surface regeneration. Later measurements of high-affinity mutants using the 10 mM HCl regeneration buffer yielded effective surface regeneration and gradients that could be globally fit.

BIAevaluation version 4.1 (Biacore Inc.) was used to analyze the results from the kinetic experiments. After double referencing to remove artifacts from nonspecific binding (*23*), simultaneous global fitting of the data for each concentration gradient to a 1:1 Langmuir model was performed to determine the association rate (k_{on}), dissociation rate (k_{off}), and dissociation constant ($K_d = k_{off}/k_{on}$). Other models, such as the two-step binding model, did not improve fit quality substantially over the 1:1 Langmuir model, which yielded high-quality fits to binding data for all mutants. For each mutant tested, at least three different Tax−HLA-A2 complex concentration gradients were used to compute the kinetic parameters and the sample standard deviation.

Simulation and Evaluation of Mutant Protein Structures. Mutant structures were simulated using the protein modeling program Rosetta (*24*), starting with the crystal structure of the wild-type A6 TCR−Tax−HLA-A2 complex (*15*) which was downloaded from the Protein Data Bank (PDB) (*25*) (entry 1AO7). Structural modeling with Rosetta was performed using the interface mutagenesis module (*24*), keeping the protein backbones fixed, and packing the mutant side chains using a rotamer-based search. Standard rotamers were augmented with extra χ_1, χ_2, and χ_3 rotamers for all residues with at least 12 neighboring residues within a 10 Å cutoff (specified by the "-ex1 -ex2 -ex3 -extrachi_cutoff 12" flags to Rosetta on the command line).

Structural models were then scored using ZAFFI, a function optimized to evaluate the binding energy changes of mutant complexes (*19*). This function uses a weighted scoring function with terms for van der Waals interaction, Lazaridis−Karplus

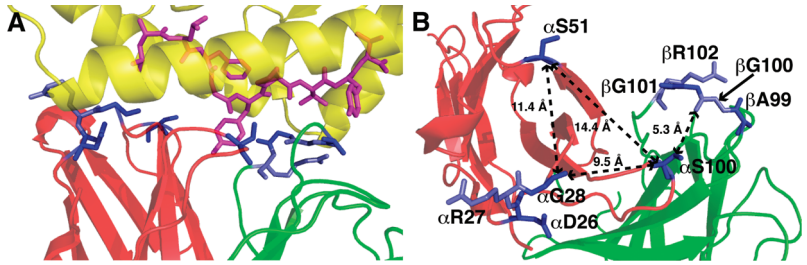

FIGURE 1: Positions of TCR mutations on the structure of the wild-type TCR−peptide−MHC complex (PDB entry 1AO7) from the side (A) and top (B; peptide and MHC not shown). The TCR α chain is colored red, the TCR *β* chain green, the MHC yellow, and the Tax peptide magenta, and mutated residues are colored blue and slate. In the right panel, residues mutated in this study are labeled by their wild-type amino acid code and position, and inter-residue distances are shown as dashed lines.

solvation (*26*), and the ACE statistical potential (*27*). For each mutant structure scored by ZAFFI, the score of the wild-type complex was subtracted to produce the predicted energetic change of the mutation.

Figures. Figures representing protein structures were generated using PyMOL (www.pymol.org), and graphs were generated using gnuplot (www.gnuplot.info).

RESULTS

Positions of TCR Mutations. To evaluate binding cooperativity in the A6 T cell receptor, we produced a set of 23 mutant TCRs with combinations of point mutations that had been measured individually with respect to their kinetics of binding to the Tax−HLA-A2 complex. The mutations in the TCR α chain are at positions 26−28, 51, and 100, located in complementarity determining regions (CDRs) 1 (residues 26−28), 2 (residue 51), and 3 (residue 100), and have wild-type residue identities of D, R, G, S, and S, respectively. The four mutated positions on the TCR *β* chain are residues 99−102 (located in CDR3), for which the wild-type sequence is AGGR. The mutations on the TCR α chain were originally identified and tested in a structure-based design study (*19*), while the four mutations on the TCR *β* chain were produced together in a high-affinity mutant in a phage display study (*20*). All of these point mutations were measured individually for kinetics by Haidar et al. and showed improved affinity, with the exception of αS100A, which led to a negligible increase in affinity, and *β*R102Q, which led to an approximately 2-fold decrease in affinity (*19*).

Figure 1 shows the location of the mutations on the structure of the wild-type TCR interface. While the αS100 and *β*A99−*β*R102 residues are close to one another near the center of the interface (with just 5.3 Å separating αS100 and *β*G100), residues αD26−αG28 and αS51 are located more on the periphery of the interface, approximately 9.5 and 14.4 Å from the αS100 residue, respectively, and 11.4 Å from each other. Among residues αD26−αG28, αG28 is the closest to the center of the interface and the mutated residues in the other CDRs.

The TCR combination mutants were expressed, folded, and tested for their kinetics of binding to the Tax−HLA-A2 complex using surface plasmon resonance, as described in Materials and Methods. Table 1 gives measured binding kinetics of the mutants, and representative binding sensorgrams for the wild-type A6 TCR and five mutants are shown in Figure 2. For the sake of simplicity, mutant TCRs with multiple α chain mutations are denoted by the amino acid identities at positions 26−28, 51, and 100, and TCRs with multiple *β* chain mutations are denoted by the amino acid identities of residues 99−102, with mutant residues in bold.

Table 1: Measured Kinetic Results for TCR Mutants Binding the Peptide−MHC Complex[a]

mutant[b]	k_{on} ($\times 10^4$ M^{-1} s^{-1})	k_{off} ($\times 10^{-3}$ s^{-1})	K_d ($\times 10^{-7}$ M)
wild-type A6	5.1 ± 0.5	108 ± 14	21 ± 3.5
α chain			
DRISA	4.6 ± 0.4	52 ± 0.7	11 ± 1.0
DRIST	2.2 ± 0.3	10 ± 0.2	4.6 ± 0.5
DRLSA	7.9 ± 0.7	70 ± 5.2	8.9 ± 1.0
DRLST	3.7 ± 0.3	14 ± 0.4	3.7 ± 0.3
DRMSA	8.0 ± 0.3	43 ± 2.5	5.4 ± 0.4
DRMST	13.8 ± 3.1	15 ± 1.6	1.1 ± 0.3
DRMMT	11.2 ± 1.4	6.6 ± 0.5	0.58 ± 0.09
DRTMT	2.7 ± 0.1	3.8 ± 0.06	1.4 ± 0.07
DFMMT	10.6 ± 0.5	11 ± 0.3	1.0 ± 0.06
DFTMT	2.3 ± 0.1	3.3 ± 0.09	1.4 ± 0.08
WFGMT	6.3 ± 0.3	1.4 ± 0.03	0.21 ± 0.01
WRMMT	2.1 ± 0.8	7.2 ± 1.2	3.4 ± 1.4
WRTMT	1.1 ± 0.3	3.0 ± 0.2	2.6 ± 0.7
WFTMT	2.0 ± 0.7	4.8 ± 0.1	2.4 ± 0.9
β chain			
AGAQ	2.1 ± 0.4	3.2 ± 0.3	1.5 ± 0.3
MSGR	2.8 ± 0.8	10 ± 0.8	3.6 ± 1.0
MSAR	3.6 ± 0.1	0.19 ± 0.06	0.053 ± 0.02
MSAQ	4.2	0.12	0.028
α and *β* chain			
G28T-**MSAR**	3.2 ± 0.7	0.10 ± 0.01	0.031 ± 0.007
G28T-**MSAQ**	5.0 ± 0.5	0.13 ± 0.05	0.026 ± 0.01
D26W-**MSAQ**	1.9 ± 0.1	0.045 ± 0.01	0.023 ± 0.007
WFGMS-MSAQ	3.3 ± 0.1	0.13 ± 0.02	0.04 ± 0.007
WFGMT-MSAQ	1.9 ± 0.4	0.11 ± 0.03	0.062 ± 0.02

[a]Errors calculated using the sample standard deviation of the three measured gradients. For mutant **MSAQ**, no standard deviation was obtained due to a lack of replicate measurements. Results for wild-type A6, **WFGMT**, and **WFTMT** reported previously by Haidar et al. (*19*). [b]Amino acid sequence of the mutant, with mutated residues in bold. For α chain mutations, residues 26−28, 51, and 100 are indicated, and for *β* chain mutations, residues 99−102 are indicated.

We also computed the changes in activation energies of association and dissociation, $\Delta\Delta G_{on}$ and $\Delta\Delta G_{off}$, respectively, defined in eqs 1 and 2. Such formulations have been used in previous studies to express changes in kinetic rates in energetic terms (*28*, *29*). $\Delta\Delta G_{on}$ is directly related to the ϕ value ($\phi = \Delta\Delta G_{on}/\Delta\Delta G$), which has been used to analyze the contribution of inter-residue interactions to TCR association (*30*, *31*). Figure S1 of the Supporting Information gives the $\Delta\Delta G_{on}$ and $\Delta\Delta G_{off}$ values for the measured TCR combination mutations, as well as the individual point mutations measured previously (*19*).

Measured Binding Kinetics. We measured binding kinetics for 14 combination mutations that contained mutations in the α chain alone, listed in Table 1. For the wild type and the

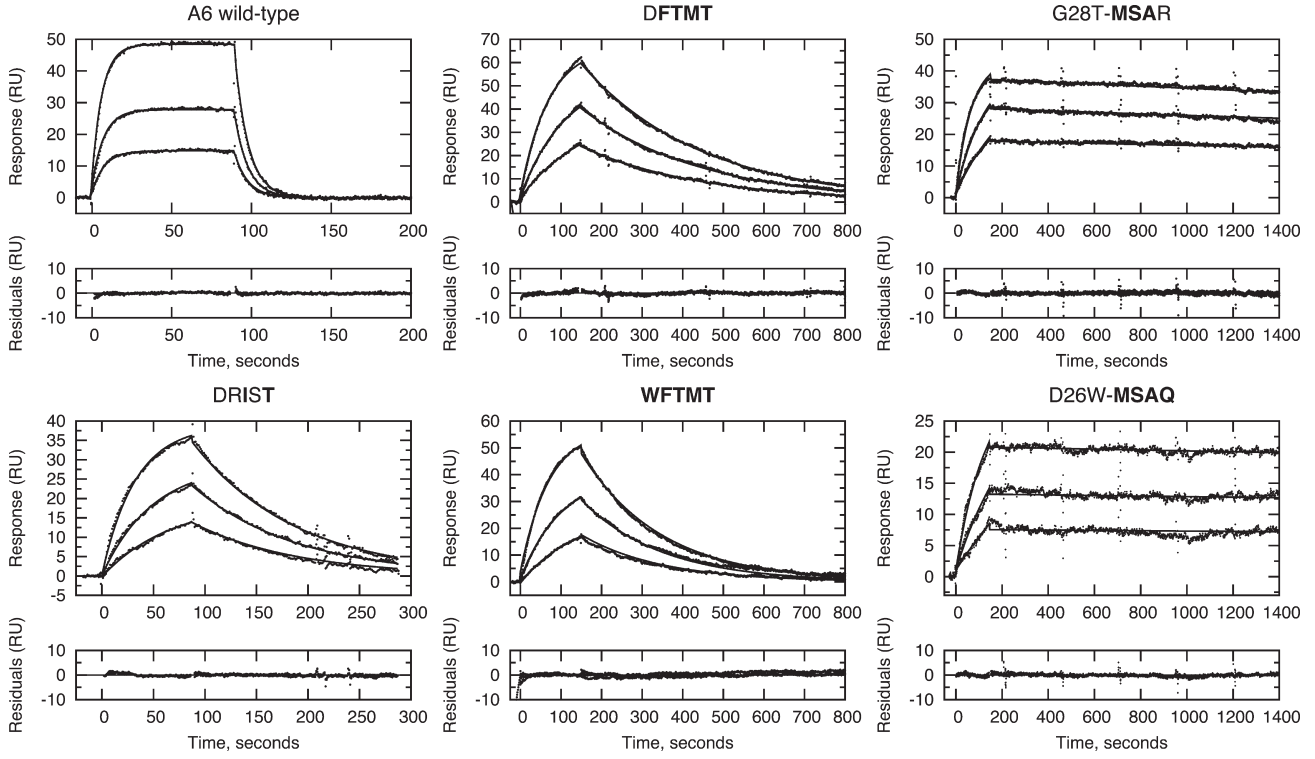

FIGURE 2: Sensorgrams for binding of the Tax−HLA-A2 complex to the wild-type A6 TCR and mutants. In each experiment, approximately 400 response units (RU) of TCR was immobilized per cell and gradients of the Tax−HLA-A2 complex were injected over the cells using serial 2-fold dilutions. Lines representing global fits of the data to the Langmuir 1:1 model are shown, and residuals are given below the sensorgrams. The following Tax−HLA-A2 complex concentrations were used: 0.84, 0.42, and 0.21 μM (wild-type A6, **DRIST**); 0.45, 0.225, and 0.1125 μM (**DFTMT**); 0.42, 0.21, and 0.115 μM (**WFTMT**); and 0.675, 0.3375, and 0.16875 μM (G28T-**MSA**R and D26W-**MSAQ**).

combination mutants **WFGMT** and **WFTMT**, the kinetic rates were reported previously (*19*). Certain other mutants of the α chain were also produced for testing (namely, **WFIMT**, **WFMMT**, **WFLMT**, **WRIMT**, and **WRLMT**), but binding could not be measured because of poor folding, likely because of the hydrophobicity of the mutant residues. Of the measured mutants, many had association rates similar to or slightly lower than the wild-type association rate of $5.1 \times 10^4\ M^{-1}\ s^{-1}$, ranging from approximately 5-fold slower (**WRTMT**) to nearly 3-fold faster (DR**MST**). Notably, the three mutants with the highest measured association rates contained the αG28M mutation, which had the highest association rate of all individual point mutations reported previously (*19*). The dissociation rates varied more than the association rates, with the largest change seen for **WFGMT**, which had a dissociation rate (and total K_d) approximately 100 times lower that of the A6 wild-type TCR. The large contribution of the dissociation rate to the total energy change (relative to the association rate) was seen in nearly all measured A6 TCR mutants (Figure S1 of the Supporting Information).

Even greater improvements in binding affinity were seen for the mutants in the TCR β chain, which were all located in the CDR3 loop. The greatest improvement was seen for the quadruple mutant **MSAQ**, identified through phage display in a previous study (*20*). Our affinity measurements for this mutant, although lacking replicate measurements, are commensurate with the values presented in that work (our measured K_d was 2.8 nM, compared with 2.5 nM reported by Li et al.). For this mutant, a modest decrease in association rate was offset by a drastic improvement in dissociation rate over that of the wild type, leading to a nearly 800-fold improvement in binding affinity. The triple mutant **MSA**R, which does not contain the βR102Q substitution, has an approximately 2-fold lower binding affinity than **MSAQ**, because of slower association and faster dissociation. Still weaker binding was observed for double mutants **MS**GR and AG**AQ**, which comprise the first two and last two point mutations in the **MSAQ** mutant, respectively, each with only approximately 10-fold binding improvement over that of the wild-type TCR.

We combined the β chain mutations with the α chain mutations from structure-based design and measured their binding kinetics, which are shown in the third portion of Table 1. These featured strong improvements (i.e., decreases) in the dissociation rates and generally slower association rates compared with that of the wild type. The combination of point mutation αD26W with the phage display mutant **MSAQ** led to improved binding, with a more than 4-fold improved dissociation rate over that of **MSAQ**, and an association rate 2-fold slower than that of **MSAQ** alone. The half-life of binding ($t_{1/2}$, equal to $\ln 2/k_{off}$) is 4.3 h for the D26W-**MSAQ** mutant, versus 6.3 s for the wild-type TCR. The SPR sensorgram for this mutant, shown in Figure 2, indicates the slow dissociation rate.

We also tested larger combinations of mutations, including the combination of α chain mutant **WFGMT** and β chain mutant **MSAQ**, which were the highest-affinity mutants from each individual chain. Surprisingly, for that combination, we observed a binding affinity (K_d) of 6.2 nM, which is greater than that of **WFGMT** alone (21 nM) but less than that of **MSAQ** alone (2.8 nM). To further probe the combinations of mutant chains, we tested the **WFGMS-MSAQ** mutant; in this case, a reversion of the αS100T mutation in **WFGMT** to wild-type serine was tested to explore the possible linking of that position to the **MSAQ** mutation in the β chain because of their spatial proximity (as shown in Figure 1). The binding affinity of **WFGMS-MSAQ** is improved slightly over that of **WFGMT-MSAQ**, primarily via

association rate improvement, indicating that the αS100T mutant was possibly hindering the association process when combined with **MSAQ**.

We noted weaker response levels in Biacore from various combinations of mutant α and *β* chains (including G28T-**MSA**R and D26W-**MSAQ** in Figure 2); we believe this is due to the reduced solubility of these TCR mutants and thus lower levels of active protein on the chip surface. To ensure the specificity of combined α and *β* chain mutants, we tested the **WFGMT-MSAQ** mutant TCR for binding to three HLA-A2-bound HIV peptides (sequences SLYNTVATL, ILKEPVHGV, and VIYQYMDDL), and no measurable binding was detected using Biacore (sensorgrams not shown). The specificities of the high-affinity mutants from each

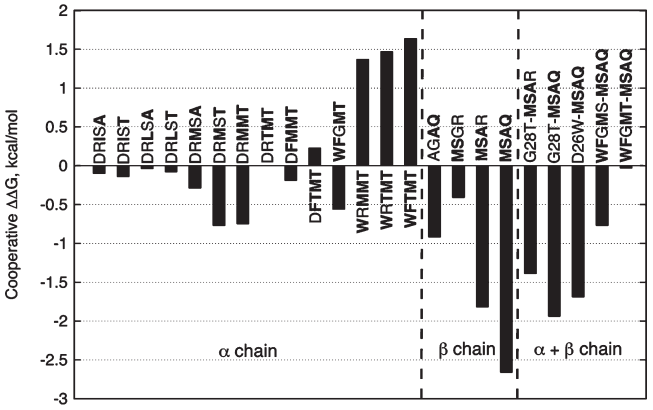

FIGURE 3: Cooperative ΔΔ*G* for combinations of TCR mutations, organized according to the chain containing the mutations. Cooperative ΔΔ*G* is defined as the difference between the measured ΔΔ*G* and the sum of ΔΔ*G* values from component point mutations measured separately.

chain, **WFGMT** and **MSAQ**, have been confirmed in previous studies (*19*, *32*).

Cooperativity of TCR Mutations. To explore the cooperative nature of the combinations of mutations presented in Table 1, we compared their measured kinetics with what would have been predicted with additivity from the individual point mutations. Figure 3 provides the cooperative ΔΔ*G*, the difference between the measured ΔΔ*G* and the sum of ΔΔ*G* values from component point mutations, for all measured combinations of TCR mutations. Table 2 gives the cooperativity in terms of total binding energy (ΔΔ*G*) as well as $\Delta\Delta G_{on}$ and $\Delta\Delta G_{off}$. To further illustrate the nonadditive and kinetic trends observed among the mutations, Figure 4 contains scatter plots of additive versus measured ΔΔ*G* values for all combinations of TCR mutants. Figure 4 indicates that, for the tested TCR mutants, the cooperativity is largely seen in the association rate (Figure 4B), whereas the dissociation rate is responsible for the anticooperativity (Figure 4C).

α *Chain Cooperativity*. While many mutants were additive, there are several instances of cooperativity and anticooperativity among the combination mutations in the α chain. Using a cooperativity cutoff for ΔΔ*G* of less than −0.5 kcal/mol [also employed by Moza et al. (*5*)], there is one cooperative mutant that contains only two mutant residues (DR**MST**). It has the point mutations αG28M and αS100T, and a cooperativity of −0.77 kcal/mol, primarily due to the association rate. As noted in Figure 1, in the structure of the wild-type TCR bound to the Tax−HLA-A2 complex these residues are not adjacent and are separated by more than 9 Å. All other measured mutants at those two positions, including I, L, and T for αG28 (DR**IST**, DR**LST**, and DR**TST**) and A for αS100 (DR**ISA**, DR**LSA**, DR**TSA**, and DR**MSA**), did not show any significant cooperativity. The degree of cooperativity seen in DR**MST** persists with the addition of the

Table 2: Binding Energies and Cooperativity for Measured TCR Mutations[a]

	CDR1α			CDR2α	CDR3α	CDR3*β*				measured binding			cooperativity[b]		
mutant	α26	α27	α28	α51	α100	*β*99	*β*100	*β*101	*β*102	ΔΔ*G*	$\Delta\Delta G_{on}$	$\Delta\Delta G_{off}$	ΔΔ*G*	$\Delta\Delta G_{on}$	$\Delta\Delta G_{off}$
DR**ISA**	D	R	**I**	S	**A**	A	G	G	R	−0.38	0.06	−0.44	−0.11	−0.10	−0.01
DR**IST**	D	R	**I**	S	**T**	A	G	G	R	−0.91	0.49	−1.40	−0.16	−0.02	−0.14
DR**LSA**	D	R	**L**	S	**A**	A	G	G	R	−0.51	−0.26	−0.25	−0.04	−0.13	0.09
DR**LST**	D	R	**L**	S	**T**	A	G	G	R	−1.03	0.20	−1.23	−0.08	−0.02	−0.06
DR**MSA**	D	R	**M**	S	**A**	A	G	G	R	−0.81	−0.26	−0.55	−0.29	0.00	−0.29
*DR**MST***	D	R	**M**	S	**T**	A	G	G	R	−1.77	−0.59	−1.18	−0.77	−0.68	−0.09
*DR**MMT***	D	R	**M**	**M**	**T**	A	G	G	R	−2.12	−0.46	−1.66	−0.75	−0.52	−0.23
DR**TMT**	D	R	**T**	**M**	**T**	A	G	G	R	−1.62	0.37	−1.99	0.01	0.17	−0.16
DF**MMT**	D	**F**	**M**	**M**	**T**	A	G	G	R	−1.78	−0.43	−1.35	−0.21	−0.22	0.01
DF**TMT**	D	**F**	**T**	**M**	**T**	A	G	G	R	−1.61	0.46	−2.07	0.24	0.53	−0.29
WFGMT	**W**	**F**	G	**M**	**T**	A	G	G	R	−2.72	−0.13	−2.59	−0.57	−0.67	0.10
WRMMT	**W**	R	**M**	**M**	**T**	A	G	G	R	−1.08	0.52	−1.60	1.36	0.02	1.34
WRTMT	**W**	R	**T**	**M**	**T**	A	G	G	R	−1.23	0.89	−2.12	1.47	0.25	1.22
WFTMT	**W**	**F**	**T**	**M**	**T**	A	G	G	R	−1.28	0.56	−1.84	1.64	0.19	1.45
*AG**AQ***	D	R	G	S	S	A	G	**A**	**Q**	−1.56	0.52	−2.08	−0.92	−0.56	−0.36
MSGR	D	R	G	S	S	**M**	**S**	G	R	−1.04	0.36	−1.40	−0.42	−0.27	−0.15
MSAR	D	R	G	S	S	**M**	**S**	**A**	R	−3.54	0.21	−3.75	−1.83	−1.02	−0.81
MSAQ	D	R	G	S	S	**M**	**S**	**A**	**Q**	−3.93	0.11	−4.04	−2.67	−1.60	−1.07
*G28T-**MSAR***	D	R	**T**	S	S	**M**	**S**	**A**	R	−3.87	0.27	−4.14	−1.39	−0.79	−0.60
*G28T-**MSAQ***	D	R	**T**	S	S	**M**	**S**	**A**	**Q**	−3.97	0.01	−3.98	−1.94	−1.53	−0.41
*D26W-**MSAQ***	**W**	R	G	S	S	**M**	**S**	**A**	**Q**	−4.04	0.57	−4.61	−1.71	−1.58	−0.13
WFGMS-MSAQ	**W**	**F**	G	**M**	S	**M**	**S**	**A**	**Q**	−3.71	0.26	−3.97	−0.79	−1.59	0.80
WFGMT-MSAQ	**W**	**F**	G	**M**	**T**	**M**	**S**	**A**	**Q**	−3.46	0.60	−4.06	−0.05	−1.65	1.60

[a]Mutant residues are shown in bold, and mutants with cooperative or anticooperative energetics (cooperative ΔΔ*G* < −0.5 kcal/mol or cooperative ΔΔ*G* > 0.5 kcal/mol) shown in italics. All ΔΔ*G* values given in units of kilocalories per mole. $\Delta\Delta G_{on} = RT\ln(k_{on\_wild\text{-}type}/k_{on\_mutant})$, and $\Delta\Delta G_{off} = RT\ln(k_{off\_mutant}/k_{off\_wild\text{-}type})$, with k_{on} and k_{off} equal to the association and dissociation rates, respectively. $\Delta\Delta G = RT\ln(k_{off\_mutant}k_{on\_wild\text{-}type}/k_{on\_mutant}k_{off\_wild\text{-}type}) = \Delta\Delta G_{on} + \Delta\Delta G_{off}$. [b]Cooperativity equals the difference between the measured ΔΔ*G* for the mutant and the sum of ΔΔ*G* values for the component point mutations.

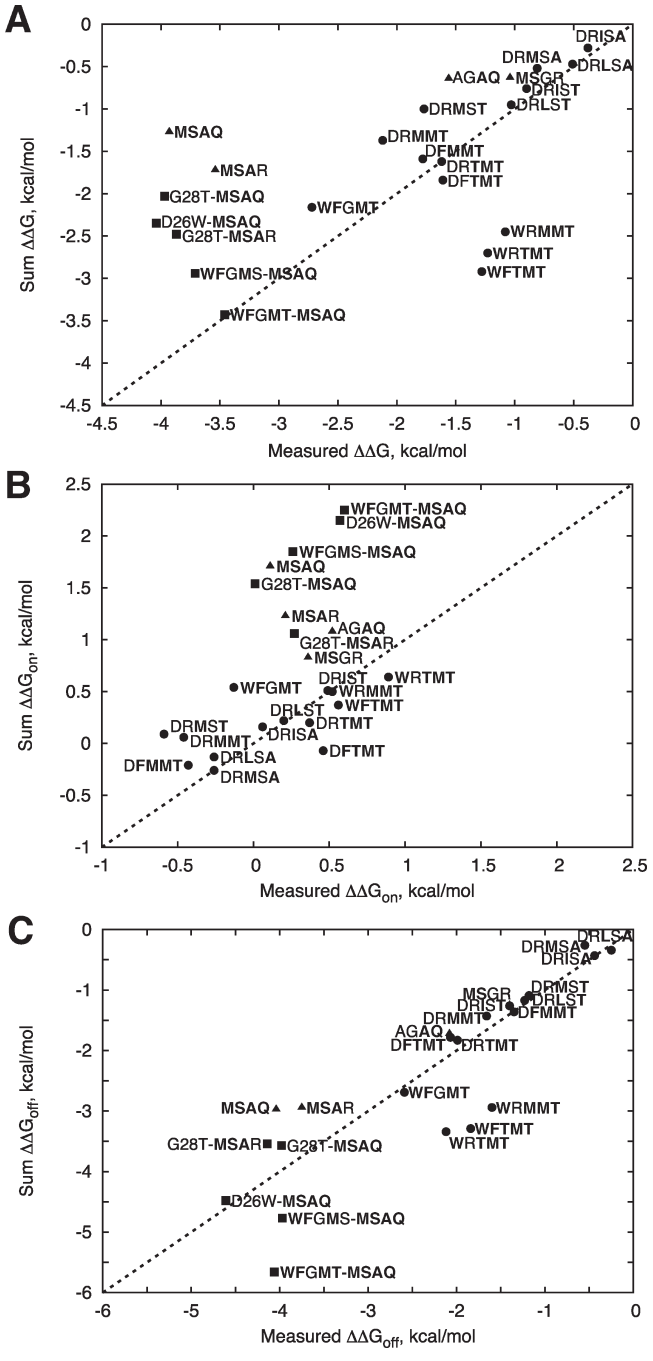

FIGURE 4: Additive vs measured binding energy change for (A) total energy ($\Delta\Delta G$), (B) association activation energy ($\Delta\Delta G_{on}$), and (C) dissociation activation energy ($\Delta\Delta G_{off}$) for 23 measured TCR mutations. Point types indicate the TCR chain containing the mutations: (●) α chain only, (▲) β chain only, and (■) α and β chains. The dashed line represents additive binding energetics. Correlations are (A) 0.56 (all points) and 0.47 (α chain only), (B) 0.46 (all points) and 0.66 (α chain only), and (C) 0.87 (all points) and 0.82 (α chain only).

αS51M mutation (DR**MMT**), suggesting that the αS51M mutation is additive in the context of the other two mutated sites. Given its distance from the other residues and location on the periphery of the interface (Figure 1), it is not surprising that the αS51M mutation behaves additively. The αS51M mutation also behaves additively when combined with the additive double mutant DR**TST** to produce the triple mutant DR**TMT**. When the αR27F mutation is combined with the triple mutant DR**MMT** (to generate D**FMMT**), the degree of cooperativity decreases from −0.75 to −0.19 kcal/mol and leads to a lower binding affinity; likewise, addition of the αR27F mutation to DR**TMT** results in slight anticooperativity in mutant D**FTMT** (leaving the binding affinity essentially the same as that of DR**TMT**). Given its proximity to αG28, it is possible that the nonadditive behavior of the αR27F mutation with the triple mutations is due to the altered backbone dynamics or conformation of CDR1α.

We explored other combinations of α chain mutations that included the point mutant αD26W, resulting in both cooperative and anticooperative energetics. The strongest binding α chain mutant, **WFGMT**, exhibited a cooperative $\Delta\Delta G$ of −0.56 kcal/mol due to the association rate, leading to a total $\Delta\Delta G$ of −2.59 kcal/mol. Given the additivity of the αS51M mutation in the context of other mutations and its distance from the CDR1 residues (13 Å from αD26 and 11.5 Å from αR27 in the wild-type structure), we reason that interactions between the αD26W mutation and the other mutant residues, αR27F or αS100T, are responsible for the cooperativity. The other combination α chain mutations, including αD26W, **WRMMT**, **WRTMT**, and **WFTMT**, showed strong anticooperativity (> 1.3 kcal/mol) due to the dissociation rate (these mutants are outliers in Figure 4A,C). As other mutants with αD26W, αS51M, and αS100T (**WFGMT**) and αG28T or αG28M, αS51M, and αS100T (DR**MMT** and DR**TMT**) do not possess anticooperative energetics, and αR27F does not increase the anticooperativity when added to **WRTMT** (in the mutant **WFTMT**), combinations of the αD26W mutation along with either αG28M or αG28T seem to be responsible for the anticooperativity. As these residues are spatially proximal in CDR1, it is possible that some steric hindrance is responsible for the anticooperativity; the structural implications of these mutant combinations will be discussed in more detail later.

β Chain Cooperativity. In contrast to the anticooperativity and additivity observed among the α chain mutants, the four mutants in the TCR β chain were all cooperative when combined. The double mutants **AG**AQ and MS**GR** both exhibited some cooperativity between the adjacent point mutations (the latter had a cooperativity of −0.41 kcal/mol which was slightly less than the threshold of −0.5 kcal/mol). Upon addition of the βG101A mutation to **MS**GR to produce **MSA**R, the cooperativity (and consequently the binding affinity) improved dramatically to −1.82 kcal/mol. The cooperativity improved further for the **MSAQ** mutant (which included βR102Q), to −2.66 kcal/mol, yielding a $\Delta\Delta G$ of −3.93 kcal/mol. While both the association and dissociation rates were responsible for the cooperativity of **MSAQ**, the association rate made a larger contribution (−1.60 kcal/mol). It is worth noting that the affinity improvement from **MSA**R to **MSAQ** is approximately equal to the improvement from βG101A to **AG**AQ, suggesting that the adjacent βG101A mutation is responsible for the cooperativity observed upon addition of βR102Q to **MSA**R. Even the sum of $\Delta\Delta G$ values from the two pairs of mutations (AG**AQ** and **MSGR**) comprising the **MSAQ** mutant (−3.48 kcal/mol) is somewhat smaller than the measured $\Delta\Delta G$ of **MSAQ** (−3.93 kcal/mol), indicating cooperativity among (in addition to within) these pairs of positions.

α and β Chain Cooperativity. Combinations of the mutant α and β chains were primarily cooperative when compared with the sum of the component point mutations. Strikingly, the association rate cooperativity of approximately −1.60 kcal/mol persists for all combinations of α chains with **MSAQ** (including the wild-type α chain), despite widely varying dissociation rate additivity. This consistency can be seen in the linear

Table 3: Nonadditive Energetics[a] between Mutant TCR Chains

	association rate			dissociation rate			total		
mutant	$\Delta\Delta G_{on}$	sum[b]	IC_Coop[c]	$\Delta\Delta G_{off}$	sum[b]	IC_Coop[c]	$\Delta\Delta G$	sum[b]	IC_Coop[c]
G28T-**MSAR**	0.27	0.04	0.23	−4.14	−4.35	0.21	−3.87	−4.30	0.43
G28T-**MSAQ**	0.01	−0.06	0.07	−3.98	−4.64	0.66	−3.97	−4.69	0.72
D26W-**MSAQ**	0.57	0.55	0.02	−4.61	−5.55	0.94	−4.04	−5.01	0.97
WFGMT-MSAQ	0.60	−0.02	0.62	−4.06	−6.63	2.57	−3.46	−6.65	3.19

[a]All values are in units of kilocalories per mole. [b]Sum of the $\Delta\Delta G$ values from the mutant α chain and mutant β chain. [c]Interchain cooperativity, defined as the difference between the measured $\Delta\Delta G$ and the sum of measured $\Delta\Delta G$ values from each mutant TCR chain.

trend of these mutants in Figure 4B and suggests that **MSAQ** is responsible for the association rate shift and dominates the association kinetics in the context of mutated α chains.

When we compared the measured kinetics with the kinetics obtained upon addition of the contributions from each mutant chain [interchain cooperativity (Table 3)], however, there is considerably less cooperativity; i.e., the measured energetic improvement is not as large as what would be expected from additivity between the individually measured mutant chains. This is most apparent for **WFGMT-MSAQ**, which would have a $\Delta\Delta G$ of −6.65 kcal/mol from additivity between chains but instead has a measured $\Delta\Delta G$ of −3.46 kcal/mol, which represents a >200-fold difference in binding affinity (K_d). The smaller and more distant mutants on the α chain became slightly more additive with the β chain mutants (though still anticooperative), with D26W-**MSAQ**, G28T-**MSAQ**, and G28T-**MSAR** having interchain cooperativities of 0.97, 0.73, and 0.43 kcal/mol, respectively. The interchain anticooperativity in Table 3 is primarily due to the dissociation rate, as with the anticooperative mutants from the α chain alone (**WRMMT**, **WRTMT**, and **WFTMT**), suggesting a context-dependent alteration of the bound state for one or both mutant chains.

Structural Modeling of Anticooperative Mutations. Previously, we utilized Rosetta (*24*) to generate structural models for individual TCR point mutations bound to the peptide and MHC, leading to considerable accuracy for predicted $\Delta\Delta G$ values for this system (*19*). After noting the anticooperativity for mutants **WRMMT**, **WRTMT**, and **WFTMT**, we investigated the structural models of these mutations.

Models for TCR mutants **WRMMT** and **WRTMT** are shown in Figure 5. Although the side chain positions of mutations αD26W, αG28M, and αG28T are identical to those in the models of the individual point mutations, surprisingly there is some side chain clash seen in the models for their combination, with less than 3 Å between non-hydrogen atoms of the two side chains. When the scoring function ZAFFI (*19*) is used to evaluate the inter-residue energetics, there is a van der Waals energetic penalty of approximately 0.95 kcal/mol due to clash between the αD26W and αG28T mutations, and 0.62 kcal/mol due to clash between the αD26W and αG28M mutations. This clash was ignored by the ZAFFI function initially, because intrachain clash was normally minimal and led to scoring function noise. Such clash is the likely reason behind the anticooperativity of mutations **WRMMT**, **WRTMT**, and **WFTMT**. The αR27F mutant (in **WFTMT**, not shown in the figure), which does not seem to affect the anticooperativity, is directed away from the TCR side chains at positions 26 and 28 on the α chain in the Rosetta models and thus is not predicted to interact with them. We also searched for similar clashes in models of the other measured A6 combination mutations and identified none.

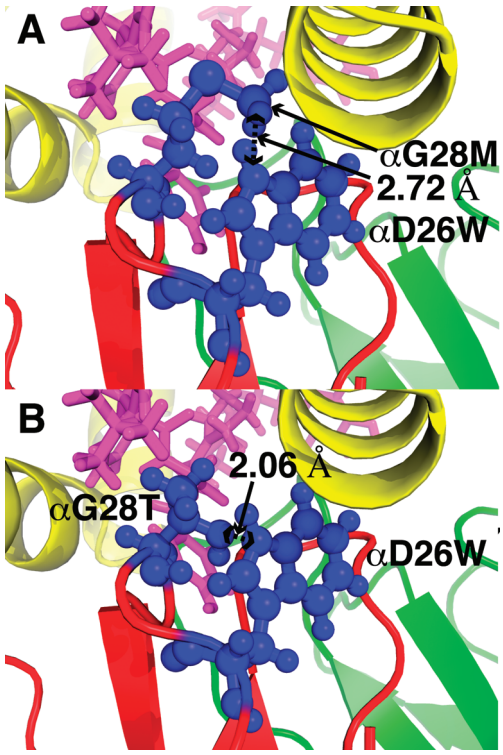

FIGURE 5: Structural models of mutated TCR α chain residues 26 and 28 in mutants **WRMMT** (A) and **WRTMT** (B), produced by Rosetta (*24*). The TCR α chain is colored red, the TCR β chain green, the peptide magenta, and the MHC yellow, and mutant residues at positions α26 and α28 are colored blue. The shortest inter-residue heavy atom distances are denoted as dotted lines.

DISCUSSION

In this study, we measured binding for combinations of mutations of a TCR that has been engineered using two methods, allowing us to characterize cooperativity within and between sets of mutations in the same binding interface. As with the results for individually engineered A6 TCR chains reported previously (*19*, *20*), the greatest improvement was seen for the dissociation rates, while the association rate did not vary substantially among TCR mutants. Many designed TCRs also have greater improvements in dissociation rate [aside from the A6 TCR, seven of nine engineered TCRs had greater dissociation rate vs association rate improvements in a recent review (*33*)], suggesting that this route of binding improvement is not unique to the A6 TCR. Suboptimal dissociation likely results from the fact that TCRs with long binding half-lives are removed *in vivo* during negative selection in the thymus. Additionally, dissociation rate improvements in the case of the designed A6 point mutants resulted in part from the design algorithm, which

stabilized the bound state and featured shape complementarity and desolvation scoring terms (*19*).

In analyzing the kinetic values from SPR, we used the simple 1:1 Langmuir binding model to obtain values of association and dissociation kinetics (and the dissociation equilibrium constant, K_d), which, given the complex nature of TCR−peptide−MHC binding, is certain to overlook molecular events taking place during the interaction process. As noted by others (*34*, *35*), protein−protein binding often occurs with a "transition state" intermediate between unbound and bound proteins, shown as AB* in eq 4 for the binding of proteins A and B:

$$A + B \underset{k_{-1}}{\overset{k_1}{\rightleftarrows}} AB* \underset{k_{-2}}{\overset{k_2}{\rightleftarrows}} AB \quad (4)$$

In eq 4, the first step is determined by diffusive and long-range electrostatic forces, while the change from the intermediate to the bound state is guided by short-range interactions and minor structural adjustments to form the bound protein complex. By using a Langmuir 1:1 binding model, intermediate states are not addressed explicitly (i.e., individual terms k_1, etc., dealing with the encounter complex are not given), and just the overall kinetic values for association and dissociation are determined. In a comprehensive mutagenesis study of the TEM-1−BLIP interaction, the authors discussed that though in reality the transition state is likely formed, if it is in a steady state and does not accumulate over time it does not need to be considered in calculating the K_d, and the 1:1 Langmuir model can be used (*34*). In the same study, it was found that SPR using the 1:1 model for analysis was accurate in determining relative $\Delta\Delta G$ values between the wild type and mutant (while less accurate for absolute binding energetic values), upon comparison of SPR to other measurement systems. In the study presented here, as with our previous report of A6 TCR point mutations (*19*), all TCR mutants measured fit well to a 1:1 Langmuir binding model, which has been used by a number of other laboratories to analyze the interaction of the TCR with the peptide−MHC complex (*17*, *30*, *36*, *37*), despite strong evidence of conformational change upon binding (*38*, *39*). Others have noted the difficulty of detecting transition state complexes using SPR for TCR recognition (*40*) and protein complexes in general (*41*), due to the temporal resolution of such techniques, leading some to utilize less direct methods such as ϕ value analysis (*30*, *31*) and analysis of kinetic cooperativity (*42*) to infer the structure and dynamics of the binding transition state.

In this study, the measured combinations of A6 TCR mutations yielded several examples of nonadditive energetics. Within the α chain, there was a notable example of cooperativity, between mutations αG28M and αS100T, due to the association rate. Nonadditivity in the association rate is said to be due to interaction between residues in the binding transition state (*41*); this has been applied in analysis of mutants of the barnase−barstar complex (*43*). In the structure of the wild-type A6 TCR bound to the Tax−MHC complex, these residues are not particularly close (they are separated by 9.5 Å based on all atoms, with the Cα atoms separated by more than 13 Å), raising the question of whether these residues are close enough to permit interaction prior to binding. Unfortunately, the structure of the unbound A6 TCR has not been crystallized, precluding an analysis of the unbound state for this system, but on the basis of data for other systems, TCRs are known to exhibit plasticity in their CDR loops upon binding to the peptide−MHC complex (*44*). A review of 12 sets of unbound and bound TCR structures revealed that the CDR3α, CDR3β, and CDR1α loops have the highest degree of average movement upon peptide−MHC binding, with average rmsds (root-mean-square distances) of 4.7, 3.8, and 2.8 Å, respectively (*39*); thus, the CDR3α loop in particular may be capable of movement closer to CDR1α in the unbound A6 TCR and its mutants.

The fact that only αG28M and αS100T mutations resulted in cooperativity, rather than the other tested pairs of mutations at those positions, seems to indicate a shift in interface architecture specific to those mutations that contradicts the notion of static modules that dictate cooperativity between interface positions. In fact, a recent study of the TEM1−BLIP interface identified a pair of mutations (E104Y and Y105N on TEM1) that resulted in a backbone movement in BLIP and a rearrangement of the interface modules observed in the crystallized mutant complex (*28*). The αG28M mutation in particular has several notable characteristics, including the fact that it has the highest association rate of the measured A6 TCR point mutations. The original energetic prediction for the $\Delta\Delta G$ of the αG28M point mutation was an outlier, where the affinity improvement was overestimated by more than 1 kcal/mol (*19*). This may indicate that the structural modeling that was used to produce the αG28M prediction (which assumed a static backbone and neighboring side chains) was incorrect, but in the context of αS100T, this conformation was achieved.

In addition to the cooperativity within individual chains, we also studied the degree of cooperativity upon combination of mutations from the different selection methods (Table 3) and, rather than simple additivity, found evidence of complex long-range interdependence. Particularly striking is the fact that the combination of the high-affinity mutations from each chain (**WFGMT-MSAQ**) yielded far less affinity than expected from the sum of $\Delta\Delta G$ values from each chain (**WFGMT** and **MSAQ**), a difference of 3.19 kcal/mol (200-fold K_d). On the basis of modeling of the α chain mutations that also show energetic and dissociation rate anticooperativity, it is possible that this is due to the mutations on each chain leading to hindrances to optimal binding. This is also supported by the fact that the level of energetic anticooperativity appears to diminish as the number of mutations on the TCR α chain becomes smaller. It worth noting that the combination of D26W on the α chain and **MSAQ** on the β chain exhibits significant anticooperativity (0.97 kcal/mol), as those positions are separated by approximately 17 Å in the wild-type complex. This suggests possible shifts in the TCR docking mode or CDR movements due to either **MSAQ** or αD26W (or both) that cannot be satisfied upon combination of these mutations. While preliminary reports of the bound **MSAQ** mutant indicate CDR3β loop and peptide residue Y5 side chain movement (*45*), it is unclear whether this occurs along with subtle α and β chain domain shifts as observed for the A6 TCR bound to a chemically modified Y5 peptide and the MHC (*38*), or more localized loop movement as observed with the V7R peptide variant and the MHC (*16*). Given the observed nonadditivity, it seems that the latter scenario is unlikely. A recently released structure of another TCR (MEL5), which shares the germ line CDR1α and CDR2α sequences with the A6 TCR (from the *TRAV12-2* gene), bound to a modified cancer epitope and HLA-A2 featured the same "α-centric" binding mode of the TCR, with very similar CDR1α conformation and antigen contacts, despite the considerable difference between the Tax and ELA peptides and the TCR CDR3α loops and β chains (*46*). This supports the

possibility that the mutant β chain (rather than the α chain) may undergo conformational change to allow CDR1α to retain its conserved binding mode, which even in the context of the CDR1α mutants retains key binding residues such as αQ30.

These results can help to inform future rational design studies that combine multiple point mutations or multiple sets of mutations. As noted previously by Midelfort and Wittrup for combinations of mutations in a high-affinity designed antibody (*47*), we found that distant, peripheral residue mutations can lead to additive binding energetics, as in the case of αS51M. However, nonadditivity is more likely when dealing with adjacent mutations, and mutations of adjacent residues to larger residues risk possible anticooperative effects (as observed upon combination of αD26W with αG28T or αG28M in this study). It is possible to rationally design cooperativity in neighboring residues, as performed by Lippow et al.; however, the authors noted that such multiple-residue designs yield a lower success rate than point mutation design (*8*), likely due to the complexity and uncertainty at the atomic level of multiple modeled residues. Finally, combinations of a large set of neighboring mutations with distant residues can lead to nonadditivity, as we observed when combining the **MSAQ** and **MSAR** mutations on the β chain with various α chain mutations. The βG101A point mutant, for example, may have led to better additivity with the single mutant or multiple mutants of the α chain as its effects may be more localized than the larger sets of β chain mutations.

In summary, we have combined kinetic measurements of a large set of combinations of mutations with *in silico* structural modeling and analysis, leading to a clearer picture of the kinetic and structural basis of cooperativity and TCR−peptide−MHC binding. Future work in crystallization of high-affinity mutants would help confirm whether loop movements and/or large-scale structural changes are responsible for cooperativity and anticooperativity within and among the chains. Additionally, further biophysical characterization of the mutants, using, for instance, isothermal calorimetry (ITC) or SPR with varying temperature points, would help to elucidate the entropic terms underlying the energetic and kinetic measurements of the TCR mutants presented in this study. The results presented here provide a data set for further exploration of cooperativity and binding affinity analysis and can help to guide future rational design and *in vitro* selection protein engineering efforts.

ACKNOWLEDGMENT

We are grateful to the Scientific Computing Facilities at Boston University, the Advanced Biomedical Computing Center at the National Cancer Institute for computing resources, Mary Ellen Fitzpatrick for computing support, and Dr. Pierre Rizkallah (Synchrotron Radiation Source, Daresbury Laboratory, Warrington, U.K.) for helpful discussions. We appreciate the help of the late Dr. Jonathan Boulter (Cardiff University School of Medicine, Heath Park, U.K.) who provided generous assistance before his untimely death.

SUPPORTING INFORMATION AVAILABLE

Binding energy change components, $\Delta\Delta G_{on}$ and $\Delta\Delta G_{off}$, for 13 point mutations from Haidar et al. (*19*) (A) and 23 combination mutations (B), organized from left to right in order of improving total binding energy ($\Delta\Delta G$). This material is available free of charge via the Internet at http://pubs.acs.org.

REFERENCES

1. Wells, J. A. (1990) Additivity of mutational effects in proteins. *Biochemistry 29*, 8509–8517.
2. Reichmann, D., Rahat, O., Albeck, S., Meged, R., Dym, O., and Schreiber, G. (2005) The modular architecture of protein-protein binding interfaces. *Proc. Natl. Acad. Sci. U.S.A. 102*, 57–62.
3. Kraich, M., Klein, M., Patino, E., Harrer, H., Nickel, J., Sebald, W., and Mueller, T. D. (2006) A modular interface of IL-4 allows for scalable affinity without affecting specificity for the IL-4 receptor. *BMC Biol. 4*, 13.
4. del Sol, A., and Carbonell, P. (2007) The modular organization of domain structures: Insights into protein-protein binding. *PLoS Comput. Biol. 3*, e239.
5. Moza, B., Buonpane, R. A., Zhu, P., Herfst, C. A., Rahman, A. K., McCormick, J. K., Kranz, D. M., and Sundberg, E. J. (2006) Long-range cooperative binding effects in a T cell receptor variable domain. *Proc. Natl. Acad. Sci. U.S.A. 103*, 9867–9872.
6. Bernat, B., Sun, M., Dwyer, M., Feldkamp, M., and Kossiakoff, A. A. (2004) Dissecting the binding energy epitope of a high-affinity variant of human growth hormone: Cooperative and additive effects from combining mutations from independently selected phage display mutagenesis libraries. *Biochemistry 43*, 6076–6084.
7. Clark, L. A., Boriack-Sjodin, P. A., Eldredge, J., Fitch, C., Friedman, B., Hanf, K. J., Jarpe, M., Liparoto, S. F., Li, Y., Lugovskoy, A., Miller, S., Rushe, M., Sherman, W., Simon, K., and Van Vlijmen, H. (2006) Affinity enhancement of an in vivo matured therapeutic antibody using structure-based computational design. *Protein Sci. 15*, 949–960.
8. Lippow, S. M., Wittrup, K. D., and Tidor, B. (2007) Computational design of antibody-affinity improvement beyond in vivo maturation. *Nat. Biotechnol. 25*, 1171–1176.
9. Sette, A., Newman, M., Livingston, B., McKinney, D., Sidney, J., Ishioka, G., Tangri, S., Alexander, J., Fikes, J., and Chesnut, R. (2002) Optimizing vaccine design for cellular processing, MHC binding and TCR recognition. *Tissue Antigens 59*, 443–451.
10. Lazoura, E., and Apostolopoulos, V. (2005) Insights into peptide-based vaccine design for cancer immunotherapy. *Curr. Med. Chem. 12*, 1481–1494.
11. Boulter, J. M., and Jakobsen, B. K. (2005) Stable, soluble, high-affinity, engineered T cell receptors: Novel antibody-like proteins for specific targeting of peptide antigens. *Clin. Exp. Immunol. 142*, 454–460.
12. Miles, J. J., Silins, S. L., and Burrows, S. R. (2006) Engineered T cell receptors and their potential in molecular medicine. *Curr. Med. Chem. 13*, 2725–2736.
13. Ashfield, R., and Jakobsen, B. K. (2006) Making high-affinity T-cell receptors: A new class of targeted therapeutics. *IDrugs 9*, 554–559.
14. Richman, S. A., and Kranz, D. M. (2007) Display, engineering, and applications of antigen-specific T cell receptors. *Biomol. Eng. 24*, 361–373.
15. Garboczi, D. N., Ghosh, P., Utz, U., Fan, Q. R., Biddison, W. E., and Wiley, D. C. (1996) Structure of the complex between human T-cell receptor, viral peptide and HLA-A2. *Nature 384*, 134–141.
16. Ding, Y. H., Baker, B. M., Garboczi, D. N., Biddison, W. E., and Wiley, D. C. (1999) Four A6-TCR/peptide/HLA-A2 structures that generate very different T cell signals are nearly identical. *Immunity 11*, 45–56.
17. Davis-Harrison, R. L., Armstrong, K. M., and Baker, B. M. (2005) Two different T cell receptors use different thermodynamic strategies to recognize the same peptide/MHC ligand. *J. Mol. Biol. 346*, 533–550.
18. Armstrong, K. M., and Baker, B. M. (2007) A comprehensive calorimetric investigation of an entropically driven T cell receptor-peptide/major histocompatibility complex interaction. *Biophys. J. 93*, 597–609.
19. Haidar, J. N., Pierce, B., Yu, Y., Tong, W., Li, M., and Weng, Z. (2009) Structure-based design of a T-cell receptor leads to nearly 100-fold improvement in binding affinity for pepMHC. *Proteins 74*, 948–960.
20. Li, Y., Moysey, R., Molloy, P. E., Vuidepot, A. L., Mahon, T., Baston, E., Dunn, S., Liddy, N., Jacob, J., Jakobsen, B. K., and Boulter, J. M. (2005) Directed evolution of human T-cell receptors with picomolar affinities by phage display. *Nat. Biotechnol. 23*, 349–354.
21. Garboczi, D. N., Utz, U., Ghosh, P., Seth, A., Kim, J., VanTienhoven, E. A., Biddison, W. E., and Wiley, D. C. (1996) Assembly, specific binding, and crystallization of a human TCR-αβ with an antigenic Tax peptide from human T lymphotropic virus type 1 and the class I MHC molecule HLA-A2. *J. Immunol. 157*, 5403–5410.
22. Garboczi, D. N., Hung, D. T., and Wiley, D. C. (1992) HLA-A2-peptide complexes: Refolding and crystallization of molecules

expressed in *Escherichia coli* and complexed with single antigenic peptides. *Proc. Natl. Acad. Sci. U.S.A. 89*, 3429–3433.
23. Rich, R. L., and Myszka, D. G. (2000) Advances in surface plasmon resonance biosensor analysis. *Curr. Opin. Biotechnol. 11*, 54–61.
24. Kortemme, T., and Baker, D. (2002) A simple physical model for binding energy hot spots in protein-protein complexes. *Proc. Natl. Acad. Sci. U.S.A. 99*, 14116–14121.
25. Berman, H. M., Westbrook, J., Feng, Z., Gilliland, G., Bhat, T. N., Weissig, H., Shindyalov, I. N., and Bourne, P. E. (2000) The Protein Data Bank. *Nucleic Acids Res. 28*, 235–242.
26. Lazaridis, T., and Karplus, M. (1999) Effective energy function for proteins in solution. *Proteins: Struct., Funct., Genet. 35*, 133–152.
27. Zhang, C., Vasmatzis, G., Cornette, J. L., and DeLisi, C. (1997) Determination of atomic desolvation energies from the structures of crystallized proteins. *J. Mol. Biol. 267*, 707–726.
28. Reichmann, D., Cohen, M., Abramovich, R., Dym, O., Lim, D., Strynadka, N. C., and Schreiber, G. (2007) Binding hot spots in the TEM1-BLIP interface in light of its modular architecture. *J. Mol. Biol. 365*, 663–679.
29. Potapov, V., Reichmann, D., Abramovich, R., Filchtinski, D., Zohar, N., Ben Halevy, D., Edelman, M., Sobolev, V., and Schreiber, G. (2008) Computational redesign of a protein-protein interface for high affinity and binding specificity using modular architecture and naturally occurring template fragments. *J. Mol. Biol. 384*, 109–119.
30. Wu, L. C., Tuot, D. S., Lyons, D. S., Garcia, K. C., and Davis, M. M. (2002) Two-step binding mechanism for T-cell receptor recognition of peptide MHC. *Nature 418*, 552–556.
31. Davis-Harrison, R. L., Insaidoo, F. K., and Baker, B. M. (2007) T cell receptor binding transition states and recognition of peptide/MHC. *Biochemistry 46*, 1840–1850.
32. Laugel, B., Boulter, J. M., Lissin, N., Vuidepot, A., Li, Y., Gostick, E., Crotty, L. E., Douek, D. C., Hemelaar, J., Price, D. A., Jakobsen, B. K., and Sewell, A. K. (2005) Design of soluble recombinant T cell receptors for antigen targeting and T cell inhibition. *J. Biol. Chem. 280*, 1882–1892.
33. Stone, J. D., Chervin, A. S., and Kranz, D. M. (2009) T-cell receptor binding affinities and kinetics: Impact on T-cell activity and specificity. *Immunology 126*, 165–176.
34. Albeck, S., and Schreiber, G. (1999) Biophysical characterization of the interaction of the β-lactamase TEM-1 with its protein inhibitor BLIP. *Biochemistry 38*, 11–21.
35. Armstrong, K. M., Insaidoo, F. K., and Baker, B. M. (2008) Thermodynamics of T-cell receptor-peptide/MHC interactions: Progress and opportunities. *J. Mol. Recognit. 21*, 275–287.
36. Borg, N. A., Ely, L. K., Beddoe, T., Macdonald, W. A., Reid, H. H., Clements, C. S., Purcell, A. W., Kjer-Nielsen, L., Miles, J. J., Burrows, S. R., McCluskey, J., and Rossjohn, J. (2005) The CDR3 regions of an immunodominant T cell receptor dictate the 'energetic landscape' of peptide-MHC recognition. *Nat. Immunol. 6*, 171–180.
37. Weber, K. S., Donermeyer, D. L., Allen, P. M., and Kranz, D. M. (2005) Class II-restricted T cell receptor engineered in vitro for higher affinity retains peptide specificity and function. *Proc. Natl. Acad. Sci. U.S.A. 102*, 19033–19038.
38. Gagnon, S. J., Borbulevych, O. Y., Davis-Harrison, R. L., Turner, R. V., Damirjian, M., Wojnarowicz, A., Biddison, W. E., and Baker, B. M. (2006) T cell receptor recognition via cooperative conformational plasticity. *J. Mol. Biol. 363*, 228–243.
39. Armstrong, K. M., Piepenbrink, K. H., and Baker, B. M. (2008) Conformational changes and flexibility in T-cell receptor recognition of peptide-MHC complexes. *Biochem. J. 415*, 183–196.
40. Gakamsky, D. M., Luescher, I. F., and Pecht, I. (2004) T cell receptor-ligand interactions: A conformational preequilibrium or an induced fit. *Proc. Natl. Acad. Sci. U.S.A. 101*, 9063–9066.
41. Schreiber, G. (2002) Kinetic studies of protein-protein interactions. *Curr. Opin. Struct. Biol. 12*, 41–47.
42. Harel, M., Cohen, M., and Schreiber, G. (2007) On the dynamic nature of the transition state for protein-protein association as determined by double-mutant cycle analysis and simulation. *J. Mol. Biol. 371*, 180–196.
43. Frisch, C., Fersht, A. R., and Schreiber, G. (2001) Experimental assignment of the structure of the transition state for the association of barnase and barstar. *J. Mol. Biol. 308*, 69–77.
44. Clements, C. S., Dunstone, M. A., Macdonald, W. A., McCluskey, J., and Rossjohn, J. (2006) Specificity on a knife-edge: The $\alpha\beta$ T cell receptor. *Curr. Opin. Struct. Biol. 16*, 787–795.
45. Sami, M., Rizkallah, P. J., Dunn, S., Molloy, P., Moysey, R., Vuidepot, A., Baston, E., Todorov, P., Li, Y., Gao, F., Boulter, J. M., and Jakobsen, B. K. (2007) Crystal structures of high affinity human T-cell receptors bound to peptide major histocompatibility complex reveal native diagonal binding geometry. *Protein Eng., Des. Sel. 20*, 397–403.
46. Cole, D. K., Yuan, F., Rizkallah, P. J., Miles, J. J., Gostick, E., Price, D. A., Gao, G. F., Jakobsen, B. K., and Sewell, A. K. (2009) Germ line-governed recognition of a cancer epitope by an immunodominant human T-cell receptor. *J. Biol. Chem. 284*, 27281–27289.
47. Midelfort, K. S., and Wittrup, K. D. (2006) Context-dependent mutations predominate in an engineered high-affinity single chain antibody fragment. *Protein Sci. 15*, 324–334.